Biosensors and Bioelectronics 182 (2021) 113172

Contents lists available at ScienceDirect

Biosensors and Bioelectronics

journal homepage: http://www.elsevier.com/locate/bios

Textile-based wearable solid-contact flexible fluoride sensor: Toward biodetection of G-type nerve agents

K. Yugender Goud [a,1], Samar S. Sandhu [a,1], Hazhir Teymourian [a], Lu Yin [a], Nicholas Tostado [a], Frank M. Raushel [b], Steven P. Harvey [c], Lee C. Moores [d], Joseph Wang [a,*]

[a] Department of Nanoengineering, University of California, San Diego, La Jolla, CA, 92093, United States
[b] Department of Chemistry, Texas A&M University, College Station, TX, 77843, United States
[c] U.S. Army Combat Capabilities and Development Command-Chemical Biological Center (CCDC-CBC), Aberdeen Proving Ground, MD, 1010, United States
[d] U.S. Army Engineer Research and Development Center, Installation and Operation Environment Program, Environmental Laboratory, 3909 Halls Ferry Road, Vicksburg, MS, 39180, United States

ARTICLE INFO

Keywords:
Textile-based wearable sensor
Solid-contact fluoride-selective electrode
G-type nerve agents
Organophosphorus acid anhydrolylase
Organophosphorus hydrolase
Diisopropyl fluorophosphate detection

ABSTRACT

Rising global concerns posed by chemical and biological threat agents highlight the critical need to develop reliable strategies for the real-time detection of such threats. While wearable sensing technology is well suited to fulfill this task, the use of on-body devices for rapid and selective field identification of chemical agents is relatively a new area. This work describes a flexible printed textile-based solid-contact potentiometric sensor for the selective detection of fluoride anions liberated by the biocatalytic hydrolysis of fluorine-containing G-type nerve agents (such as sarin or soman). The newly developed solid-contact textile fluoride sensor relies on a fluoride-selective bis(fluorodioctylstannyl)methane ionophore to provide attractive analytical performance with near-Nernstian sensitivity and effective discrimination against common anions, along with excellent reversibility and repeatability for dynamically changing fluoride concentrations. By using stress-enduring printed inks and serpentine structures along with stretchable textile substrates, the resulting textile-based fluoride sensor exhibits robust mechanical resiliency under severe mechanical strains. Such realization of an effective textile-based fluoride-selective electrode allowed biosensing of the nerve-agent simulant diisopropyl fluorophosphate (DFP), in connection to immobilized organophosphorus acid anhydrolylase (OPAA) or organophosphorus hydrolase (OPH) enzymes. A user-friendly portable electronic module transmits data from the new textile-based potentiometric biosensor wirelessly to a nearby smartphone for alerting the wearer instantaneously about potential chemical threats. While expanding the scope of wearable solid-contact anion sensors, such a textile-based potentiometric fluoride electrode transducer offers particular promise for effective discrimination of G-type neurotoxins from organophosphate (OP) pesticides, toward specific field detection of these agents in diverse defense settings.

1. Introduction

Rapidly advancing wearable sensing technology can provide innovative solutions to various limitations in healthcare via remote and continuous monitoring of human physical metrics and physiological parameters. Thereby facilitating the realization of personalized medicine (Kim et al., 2019; Min et al., 2021; Ray et al., 2019). Wearable potentiometric sensors represent an important subclass of wearable chemical sensors, enabling the real-time monitoring of ions in physiological fluids. Recent advances in potentiometric sensors have facilitated the transition from traditional rigid ion selective electrodes (ISEs), based on inner solutions, to flexible solid-contact ISEs (Hu et al., 2016; Shao et al., 2020). These developments have led to the evolution of wearable potentiometric sensors for on-body monitoring of key electrolytes in excreted biofluids such as sweat (Bandodkar et al., 2014, 2013; Gao et al., 2016; Guinovart et al., 2013; Sempionatto et al., 2017), saliva (Lee et al., 2018), and interstitial fluid (Parrilla et al., 2019). However, despite the significant progress, wearable potentiometric

* Corresponding author.
E-mail address: josephwang@ucsd.edu (J. Wang).
[1] equal first authorship.

https://doi.org/10.1016/j.bios.2021.113172
Received 30 November 2020; Received in revised form 7 February 2021; Accepted 13 March 2021
Available online 23 March 2021

sensors have been limited to a small number of ions, mostly cations, such as sodium (Bandodkar et al., 2014; Lee et al., 2018), potassium (Parrilla et al., 2019; Sempionatto et al., 2017), pH (Bandodkar et al., 2013) and ammonium (Guinovart et al., 2013), with chloride as the only reported anion (Bariya et al., 2020; Emaminejad et al., 2017; Xu et al., 2020). Lack of reports on wearable anion-selective sensors stems partly from the different ion transduction mechanism required for such anion sensors, where, unlike in cation-selective electrodes, common p-type conductive polymers, such as poly (3-octhylthiophene) (POT), cannot be readily employed as ion-to-electron transducers (Bobacka, 2006, 1999; Mousavi et al, 2009, 2011). This reflects the redox capacitive cation sensing mechanism for such conductive polymers, which has been shown to be energetically unfavorable when coupled to the extraction of a hydrophilic anion into the selective membrane (Yuan et al., 2015). In this regard, several research groups have demonstrated the advantages of employing carbon nanomaterials, such as carbon nanotubes (CNTs) and graphene, as double layer capacitive ion-to-electron transducers in solid-contact anion sensors (Garland et al., 2018; Hassan et al., 2019; Liu et al., 2020; Parra et al., 2009; Yuan et al., 2015). However, the rigid and/or bulky design of the constituent electrodes precluded the translation of these anion sensors onto flexible and/or wearable platforms. Hence, expanding the scope of wearable anion-selective sensors from solely chloride sensing platforms to other important anions is vital for a wide variety of applications.

Although the major focus of wearable chemical sensors has been on developing wearables for healthcare and fitness applications, their use in detecting chemical threats or scanning security hazards in the wearer's ambient environment has recently received increasing attention in connection to diverse security, forensic and defense scenarios (Hubble and Wang, 2019; Windmiller and Wang, 2013). In this regard, fluoride ion is an important target anion associated with extremely toxic fluoride-containing G-type chemical warfare neurotoxins, such as soman and sarin. These organophosphate compounds (OPs) can rapidly paralyze the central nervous system through disruption of the natural activity of the neurotransmitter-associated enzyme acetylcholinesterase and the resultant accumulation of acetylcholine in neurosynapses (Goud et al., 2020). Fluorine-containing OPs can undergo biocatalytic hydrolysis reaction in the presence of enzymes that can cleave their P–F bond (*i.e.* organophosphorus hydrolase (OPH) and organophosphorus acid anhydrolase (OPAA)), resulting in the liberation of fluoride ions (Kirsch et al., 2013). Several studies on either wild-type or the genetically-modified mutants of OPH and OPAA enzymes (also known as phosphotriesterases) have demonstrated their capability to perform catalytic defluorination of G-type nerve agents (Bae et al., 2018; Kirsch et al., 2013; Simonian et al., 2001; Tsai et al., 2012). In particular, the distinct substrate affinity of OPAA makes it extremely attractive for selective detection of fluorine-containing neurotoxins. When coupled to a fluoride recognition system, such biocatalytic ability offers considerable promise toward efficient discrimination of G-type nerve agents versus common OP pesticides.

However, developing fluoride-selective sensors is very challenging due to the inherent hydrophilic nature of fluoride ions, which mandates the presence of highly selective ionophores to offset the Hofmeister series and enable efficient fluoride extraction into the hydrophobic membrane of the electrode (Kang et al., 2007; Perdikaki et al., 2002). Another challenge arises from the pH incompatibility between the enzyme and the fluoride ionophore, as fluoride ionophores commonly rely on highly acidic pH which is far from the neutral/slightly basic pH needed for optimum enzyme activity (Goud et al., 2020; Kang et al., 2010; Mitchell-Koch et al., 2006). In the absence of a reliable fluoride sensor, pH-selective sensors were commonly merged with the immobilized OPH or OPAA enzyme for monitoring the pH changes resulting from the liberation of protons (along with fluoride ions) during the hydrolysis of fluorine-containing OP agents (Mishra et al., 2018; Simonian et al., 1999, 2004). However, this strategy is subject to major challenges as all types of OPs release protons upon hydrolysis reaction and the detection sensitivity can be drastically affected by the buffering capacity of the target analyte sample (Ramanathan et al., 2010).

In this work, we demonstrate the first example of a wearable, textile-based solid-contact fluoride sensor toward the selective recognition and biodetection of fluorine-containing G-type nerve agents (Fig. 1). Textile-based wearable sensors have recently received growing attention, owing to the major role of textiles in our daily life and to their favorable elastomeric properties. Versatile textile substrates allow contact between the sensor and the body, while their extensive surface area enables the compact integration of associated electronic components (Bujes-Garrido and Arcos-Martínez, 2017; Parrilla et al., 2016; Wang et al., 2018; Xu et al., 2020). A key attribute of wearable textile-based sensors is the ability to withstand extreme mechanical deformations without affecting their analytical performance. To impart the desired robustness and mechanical resiliency to our new potentiometric sensors, we employed here a unique dielectric confinement strategy to reinforce the serpentine-based stretchable design of the electrodes. The combination of a fluoride-selective organotin-based recognition ionophore in the polymeric membrane to selectively chelate the fluoride anion (with each of the two central Sn atoms) and carboxyl-functionalized multi-walled carbon nanotubes as ion-to-electron transducer, along with careful optimization of the sensor preconditioning parameters resulted in an attractive near-Nernstian sensitivity and highly reliable fluoride response. Solving the challenge of an effective on-body fluoride sensor has opened the door to the realization of selective potentiometric biosensing of G-type nerve agents in connection to immobilized OPH or OPAA enzymes. The resulting textile-based nerve-agent biosensor is easily interchangeable and has been coupled with a miniaturized potentiostat that enabled the wireless detection of the DFP surrogate compound of G-type neurotoxins. The new wearable platform holds considerable promise for alerting soldiers and civilians rapidly regarding a potential chemical attack.

2. Experimental

All experimental details and procedures including-materials and instrumentation employed, design and fabrication of textile-based electrodes, fluoride sensor optimization protocol, mechanical resilience analyses, fluoride sensor cocktails immobilization, organophosphorus acid anhydrolase (OPAA) and organophosphorus hydrolase (OPH) enzyme immobilizations, corresponding reagent layers, potentiometric fluoride sensing and DFP biosensing experiments have been described in the Supplementary Information.

Safety Note: DFP biosensing experiments, including solution preparation and potentiometric analysis were carried out with extreme caution, owing to the high toxicity and potentially hazardous effects of DFP exposure. The stock DFP solution was always stored inside a screw-cap microcentrifuge tube and its diluted secondary solutions were stored in 15 mL centrifuge tubes. To ensure moisture-free conditions during DFP storage, an ample amount of molecular sieves was stored alongside the DFP solution. The DFP dilutions were performed by using anhydrous isopropyl alcohol (IPA) solution (99.5%) to minimize the aqueous exposure to DFP. For safety precautions, the DFP solution preparation and biosensing experiments were carried out inside a fume hood and the scientist wore two layers of gloves to lower the risk of direct skin contact. Continuous N_2 gas flow was used while preparing the diluted secondary solutions of DFP. The DFP-contaminated solid waste such as-gloves, micropipette tips, centrifuge tubes, paper wipes and textile-based DFP biosensors were appropriately decontaminated by immersing them in 0.1 M NaOH solution after use.

3. Results and discussions

3.1. Textile-based solid-contact fluoride sensing

Toward the ultimate goal of on-body detection of G-type nerve

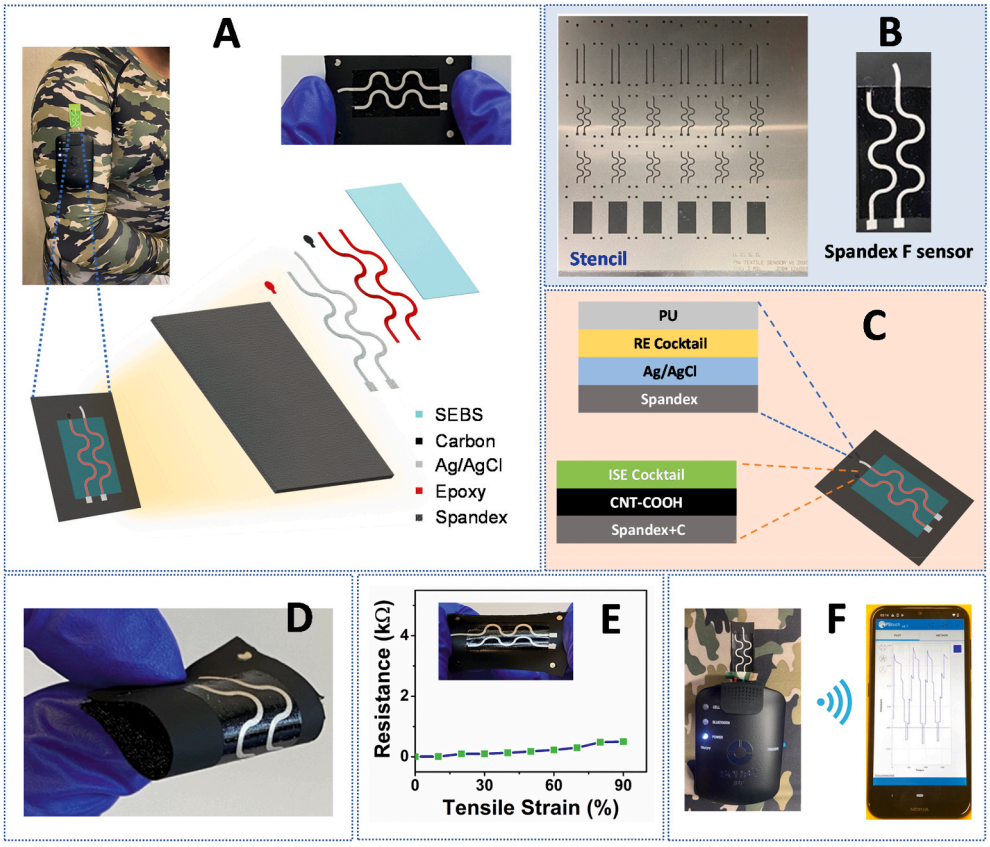

Fig. 1. Flexible and stretchable textile-based solid-contact potentiometric fluoride sensor. A. Schematic representation of screen printing the spandex fluoride sensor. B. Real image of stencil design for screen printing the sensor. C. Schematic of the modification protocol used for fabricating the solid-contact spandex fluoride sensor. D. Image of bending the spandex fluoride sensor. E. Mechanical resilience analysis of the spandex-printed electrodes. F. Spandex fluoride sensor coupled with a miniaturized, portable potentiostat and wireless interface to a nearby smartphone.

agents, we initially developed the first textile-based wearable potentiometric sensor for selective recognition of fluoride anions. G-type nerve agents yield fluoride anions upon cleavage of their P–F bonds in the presence of a suitable enzyme. Accordingly, we introduced a flexible and stretchable textile-based solid-contact fluoride sensor that could be directly screen printed on the Soldier's clothing (*i.e.* camouflage Gore-Tex coated textile) or could be easily transferred onto the Soldier's clothing. Fig. 1A illustrates the schematic representation of screen printing the spandex fluoride sensor, followed by integration of the textile-based sensor with a miniaturized portable potentiostat for wireless data transmission. The printing process was performed on the surface of a spandex textile (gray color) by first printing the Ag/AgCl ink layer (silver color) as the serpentine traces, serving as connection pads and as the RE. This was followed by printing the carbon ink layer (black color) as the WE area and its connecting trace over the adjoining Ag/AgCl serpentine trace. Printing of Gorilla epoxy (red color) involved three layers on top of the Ag/AgCl serpentine traces and one layer underneath the area designated for the carbon ink. The incorporation of Gorilla epoxy afforded dielectric confinement to the sensor design and thereby improved its mechanical resilience (Yin et al., 2018). In the final step, the insulation layer was printed by using a layer of styrene-ethylene-butylene-styrene copolymer (SEBS, light blue color) elastomer formulation. This layer secures the dielectric separation of the serpentine traces to rule out sensor short-circuits and was also useful for further enhancing the mechanical integrity of the Gorilla epoxy-confined sensor traces (Yin et al., 2021). Fig. 1B presents an image of the stencil design used for the screen-printing process, along with a real picture of the obtained spandex fluoride sensor. Fig. 1C schematically illustrates the composition of the textile-based solid--contact fluoride sensor. This schematic presents the modification protocol used for the sensor fabrication process. The WE of the spandex fluoride sensor was first modified with an intermediate layer of carboxyl-functionalized MWCNTs (CNT-COOH), followed by modification with a fluoride ion-selective membrane cocktail (comprising an organotin-based ionophore, polyvinyl chloride (PVC) dielectric matrix, potassium tetrakis (4-chlorophenyl)borate (KTpClPB) ion exchanger and bis(2-ethylhexyl) sebacate (DOS) plasticizer). In the case of the RE, it was first modified with a reference cocktail solution (comprising polyvinyl butyral (PVB) and NaCl), followed by a layer of polyurethane (PU) to minimize the leaching of chloride ions. Fig. 1D illustrates the real image of 180° bending of the spandex fluoride sensor during mechanical resiliency studies. The Dartex Exoskin®-coated spandex textile was chosen in this work owing to its superior flexibility and stretchability, compared to conventional textile substrates, along with its superior water resistance and abrasion resistance. These properties play a key role toward achieving high mechanical resiliency of the textile-based sensor under dynamic stretching and bending conditions. Fig. 1E depicts the mechanical resiliency analysis of the spandex printed electrodes. The uniaxial stretching experiments were conducted on a tensile testing machine, while sequentially changing the tensile strain from 10% to 90%, at a constant strain rate of 2 mm/s and over 25 strain cycles. The spandex fluoride sensor exhibited minimal resistance increase up to 90% tensile strain. The resistance gradually increases from 14 Ω (R_0) under 0% tensile strain to 110 Ω (R_{90}) under 90% tensile strain, which indicates good stretchability of the spandex fluoride sensor. Fig. 1F illustrates the real image of a spandex fluoride sensor coupled with a wearable potentiostat for Bluetooth-enabled wireless interfacing with a nearby smartphone. This wearable textile-based fluoride sensing approach enables the real-time electroanalyses of fluorine-containing analytes (like G-type nerve agents), directly from a nearby smartphone.

3.2. *Optimization of pre-incubation time, pre-incubation concentration and working electrode-intermediate layer*

The application of wearable textile-based sensors for defense

applications (especially warfare) necessitates their unobtrusive integration with the uniforms of military personnel. In consideration of the diverse uniforms worn within the military, we demonstrate the flexibility of the screen-printing technology for fabricating the textile-based fluoride sensors, which enabled their reproducible and reliable printing on various types of spandex-based substrates (Fig. 2D). Incorporation of ion-to-electron transducers as intermediate layers of solid-contact ISEs has been shown to provide an effective sensing performance, including near-Nernstian sensitivity, reproducibility, reversibility, pH resiliency, response time, medium- and long-term stability of potentiometric sensors (Crespo et al., 2008; Hu et al., 2016; Liu et al., 2019; Parra et al., 2009; Yuan et al., 2015). Bobacka's group pioneered the use of conductive polymers as redox capacitive transducer layers for potentiometric ion sensing (Bobacka, 2006; Mousavi et al., 2009). However, the groups of Bakker, Crespo and Rius subsequently elucidated the unique advantages of other carbon-based nanomaterials, particularly SWCNTs (Crespo et al., 2008), followed by carboxyl-functionalized MWCNTs (Parra et al., 2009) and finally, lipophilic MWCNTs (Yuan et al., 2015) as robust double layer capacitive transducer layers with highly-improved pH resilience, O_2 insensitivity, light insensitivity and minimal water layer formation versus the previously employed redox capacitance-based conductive polymers. Accordingly, we have investigated the relative impact of two types of intermediate layers, including CNT and CNT-COOH versus the bare SPCE. The impact of these layers on the fluoride sensing performance has been assessed in terms of the response drift [Fig. 2A (a-c)] and the medium-term (1 h) response stability [Fig. 2A (d)] of the solid-contact spandex fluoride sensor. In agreement with earlier studies on potentiometric anion sensors, the CNT-COOH intermediate layer led to an improved near-Nernstian sensitivity (59.2 mV/dec) versus that of bare SPCE (56.4 mV/dec), while being comparable to that of CNT (58.0 mV/dec) (Crespo et al., 2008; Parra et al., 2009; Yuan et al., 2015). This behavior can be attributed to the significantly lowered charge-transfer resistance upon employing the above intermediate layers versus the bare SPCE, which facilitates the ion-to-electron transduction mechanism for improved ion sensitivity (Crespo et al, 2008, 2009). The superiority of the CNT-COOH intermediate layer was further substantiated by the improved medium-term stability (*i.e.* lower fluoride response drift) versus those of CNT and bare SPCE. This behavior has been previously attributed to the higher low-frequency capacitance of CNT-COOH, followed by that of CNT and bare SPCE (Parra et al., 2009; Yuan et al., 2015). Hence, we selected CNT-COOH as the optimal intermediate layer for fabricating the solid-contact spandex-based fluoride potentiometric sensor.

The preconditioning parameters, particularly pre-incubation solution concentration and pre-incubation time, can have a profound impact on the performance of the potentiometric fluoride sensor (Goud et al., 2020; Hu et al., 2016). Hence, we optimized each of these two preconditioning parameters after selecting the optimal WE intermediate layer for the spandex fluoride sensor. First, we utilized two pre-incubation fluoride solution concentrations, 10 mM and 40 mM,

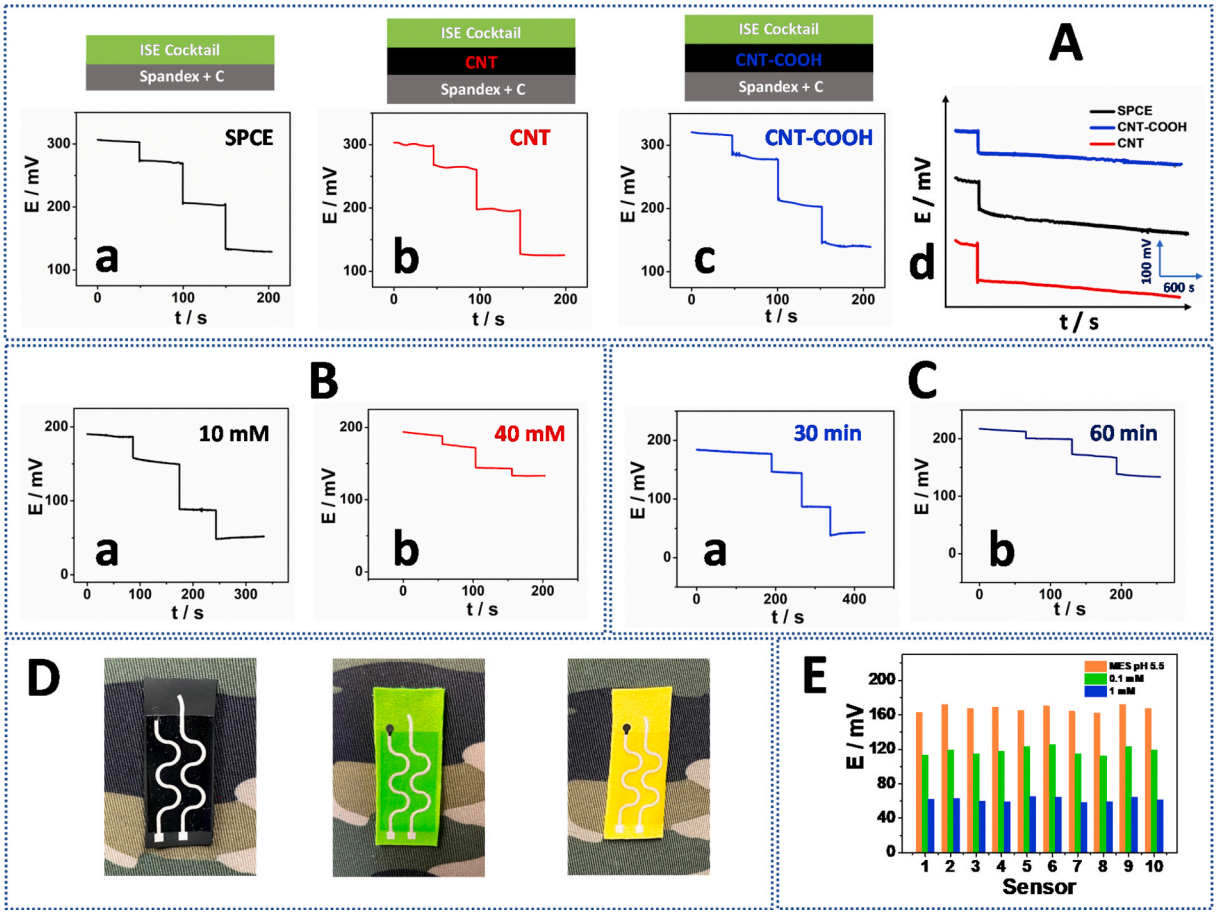

Fig. 2. Optimization of the working electrode-intermediate layer and preconditioning parameters for the textile-based potentiometric fluoride sensor. A. Optimization of the fluoride sensing performance by employing different intermediate layers- (a) Bare SPCE, (b) CNT, (c) CNT-COOH and (d) 1 h response stability analysis in 10 mM NaF sample solution with respective intermediate layers. B. Optimization of the pre-incubation solution concentration with (a) 10 mM NaF and (b) 40 mM NaF at 30 min pre-incubation time. C. Optimization of the pre-incubation time at (c) 30 min and (d) 60 min using a 10 mM NaF sample solution. D. Images of the screen-printed fluoride sensor on various spandex substrates. E. Reproducibility study of the textile-based solid-contact fluoride sensors (n = 10) while sensing fluoride concentrations of 0, 0.1 and 1 mM. Experiments were carried out in MES buffer solution (10 mM, pH 5.5).

respectively, to determine their impact on the fluoride sensing performance using a 30 min pre-incubation time. As shown in Fig. 2B, pre-incubation in the 10 mM fluoride solution resulted in a favorable near-Nernstian sensitivity of the fluoride response whereas, pre-incubation in the 40 mM fluoride solution led to a diminished fluoride response. Next, two pre-incubation times (30 min and 60 min) were examined to determine their impact on fluoride sensing performance along with the 10 mM pre-incubation fluoride solution. As shown in Fig. 2C, a pre-incubation time of 30 min offered favorable near-Nernstian sensitivity of the fluoride response, whereas the 60 min incubation significantly diminished the fluoride response. Accordingly, we selected the optimal preconditioning parameters for the spandex fluoride sensors as 30 min pre-incubation in 10 mM NaF solution (in 10 mM MES, pH 5.5). It is also important to note that an additional time interval of 5 min was required to stabilize the standard open-circuit potential (E°) of the spandex fluoride sensor prior to commencing each fluoride sensing experiment. The excellent performance of the spandex fluoride sensors can be further appreciated from the reproducibility data presented in Fig. 2E, where the open-circuit potential was measured at three different fluoride concentrations of 0, 0.1 and 1 mM, across a batch of 10 sensors (average RSD = 2.84%, n = 3 × 10).

3.3. Mechanical resilience analyses of the textile-based fluoride sensor

The realization of a robust, textile-based wearable fluoride sensor was facilitated via a sequential optimization of the sensor design. First, serpentine traces of Ag/AgCl ink were chosen to incorporate design-induced stretchability in the sensor design (Bandodkar et al., 2016). Next, Gorilla epoxy was utilized to afford dielectric confinement to the sensor design for improved mechanical resilience. Interestingly, this confinement led to a significant increase in the sensitivity of the resultant textile-based fluoride sensor (Fig. S1). The fluoride sensitivity rose from 44.67 mV/decade before confining with the dielectric, to a near-Nernstian 58.67 mV/decade with dielectric confinement. This improvement can be attributed to the improved pattern uniformity of

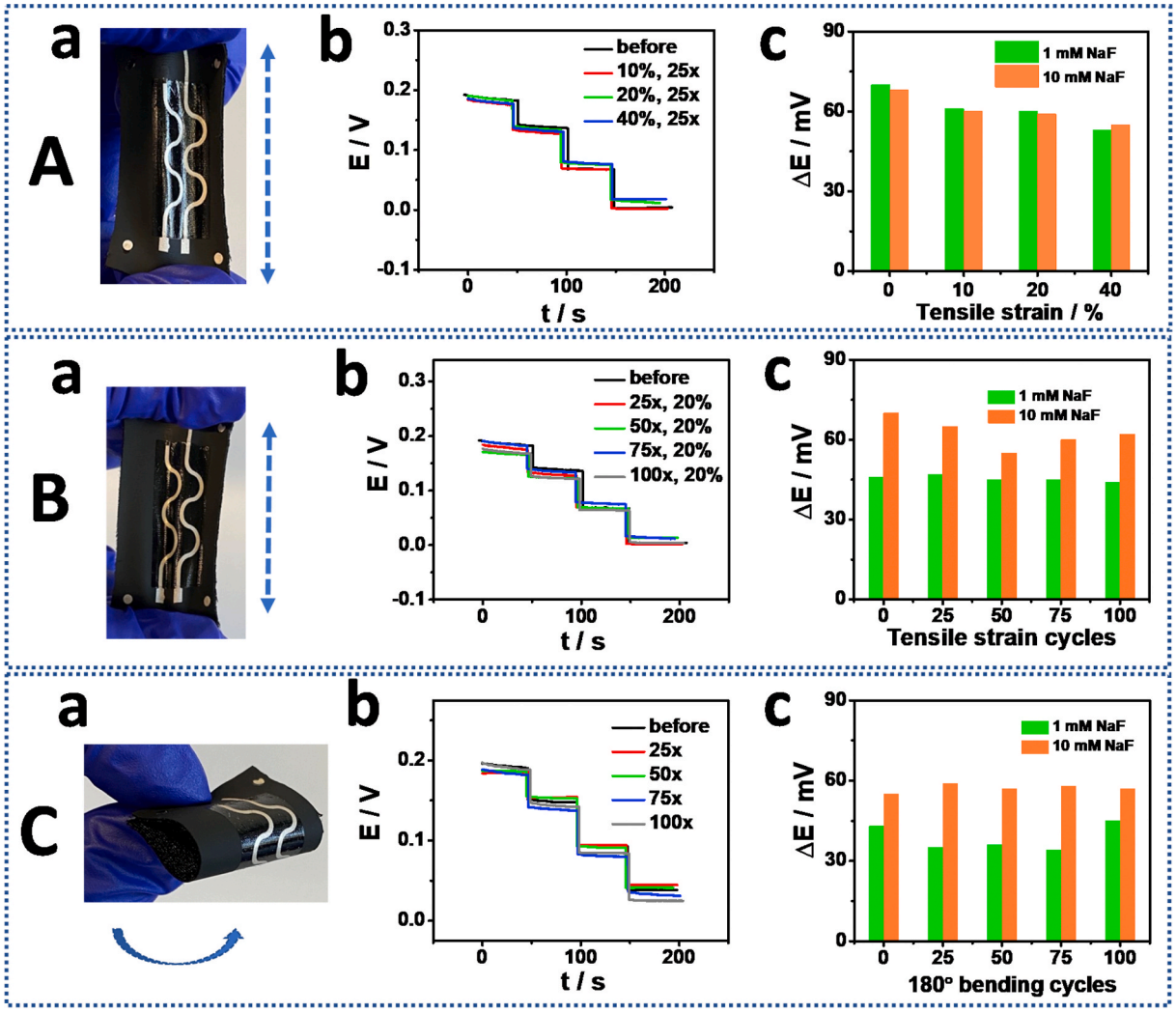

Fig. 3. Mechanical resilience analyses of the spandex fluoride sensor.A. Sensor performance with constant uniaxial tensile strain cycles - a) Image of spandex fluoride sensor under tensile strain, (b) Sensing response of spandex fluoride sensor within 0.1–100 mM concentration after 25 tensile strain cycles each of increasing tensile strain (10–40%), (c) Comparison of sensing response of spandex fluoride sensor at 1 and 10 mM concentrations after 25 tensile strain cycles each of increasing tensile strain (10–40%). B. Spandex fluoride sensor performance with constant uniaxial tensile strain - a) Image of spandex fluoride sensor under tensile strain, (b) Sensing response of spandex fluoride sensor within 0.1–100 mM concentration after increasing cycles (25–100x) of 20% tensile strain, (c) Comparison of sensing response of spandex fluoride sensor at 1 and 10 mM concentrations after increasing cycles (25–100x) of 20% tensile strain. C. Spandex fluoride sensor performance with bending - a) Image of spandex fluoride sensor under 180° bending, (b) Sensing response of spandex fluoride sensor within 0.1–100 mM concentration range after increasing cycles (25–100x) of 180° bending; (c) Comparison of sensing response of spandex fluoride sensor at 1 and 10 mM concentrations after increasing cycles (25–100x) of 180° bending.

the screen-printed carbon ink, owing to the underlying Gorilla epoxy confining layer (Yin et al., 2018). To evaluate the mechanical resiliency of the optimal spandex fluoride sensor, we critically evaluated the fluoride potentiometric response under varying degrees of uniaxial stretching and bending that exceed those expected during daily activity. Fig. 3A presents the impact of increasing uniaxial tensile strain (from 10 to 40%) on the fluoride sensing performance of the spandex fluoride sensor, for a constant 25x strain cycles. It is evident in Fig. 3A (b) that there was no appreciable increase in fluoride response drift with increasing tensile strain (RSD = 6.48%, n = 5). Such resiliency reflects the mechanical robustness of the CNT-COOH intermediate layer and its contact with the underlying carbon-based WE (Parra et al., 2009; Yuan et al., 2015). Further, Fig. 3A (c) examines the impact of increasing uniaxial tensile strain on the fluoride response at two concentrations of fluoride (1 and 10 mM). There was nearly a 15% overall reduction in fluoride sensitivity with increasing tensile strain from 0 to 40%, which can be attributed to the limited stretchability of the WE and RE cocktails (Bandodkaret al., 2014; Parrilla et al., 2016). It is important to note that other stretchable alternatives of carbon and Ag/AgCl inks (see section S1.2.) were explored but there was no appreciable improvement in the mechanical resilience of the spandex fluoride sensor. Fig. 3B presents the impact of increasing cycles of 20% uniaxial tensile strain (from 25–100x) on the fluoride sensing performance. It is evident from Fig. 3B (b) that only a negligible change in the fluoride response is observed with these increasing strain cycles (RSD = 4.27%, n = 5). Such behavior substantiates the high mechanical robustness of the CNT-COOH intermediate layer and its stable contact with the underlying carbon-based WE (Parra et al., 2009; Yuan et al., 2015). Fig. 3B (c) further illustrates the effect of increasing uniaxial tensile strain cycles on the fluoride response at two fluoride concentrations (1 and 10 mM). While the response for 1 mM fluoride remains highly stable throughout these cycles, a small (10%) decrease is observed for the 10 mM fluoride solution under these repeated severe strains. Fig. 3C examines the influence of increasing 180° bending cycles (from 25–100x) on the performance of the spandex fluoride sensor. Similar to the uniaxial stretching experiments, it is evident from Fig. 3C (b) that the textile fluoride sensor maintains its attractive performance during and after these 100 180° bending cycles (RSD = 7.92%, n = 5). Lastly, Fig. 3C (c) presents the impact of increasing 180° bending cycles on the fluoride response at two fluoride concentrations (1 and 10 mM). The response for 10 mM fluoride remains highly stable throughout these repeated strains while that of 1 mM solution increases 7% after the 100th cycle. Overall, the data of Fig. 3 clearly indicate that the new solid-contact fluoride sensor displays high resiliency against common mechanical deformations.

3.4. Analytical performance of the textile-based all-solid-state fluoride sensor

The performance of the solid-contact spandex fluoride sensor was investigated for the detection of fluoride anions. These experiments were carried out with the optimal fluoride sensor design, comprising the confining layers of Gorilla epoxy (Fig. S1), along with the CNT-COOH intermediate layer on the WE (Fig. 2B). Further, these experiments included development of the optimal sensing parameters, particularly a pre-incubation NaF solution concentration (10 mM), pre-incubation time (30 min) and a pH 5.5 MES buffer (Goud et al., 2020). To examine the concentration dependence of the new textile fluoride sensor, we recorded the potential response over the 0.1–100 mM NaF [Fig. 4A (a)] and 2–22 mM [Fig. 4A (b)] concentration ranges. As illustrated in Fig. 4A, the spandex fluoride sensor displays a near-Nernstian response, with a fluoride sensitivity around 59 mV/decade over both concentration ranges. The respective calibration plots are presented as the insets; corresponding calibration equations of $E = -58.67 \log_{10}[NaF] + 68.78$ mV, $R^2 = 0.978$ for Fig. 4A(a), inset; and $E = -58.98 \log_{10}[NaF] + 86.97$ mV, $R^2 = 0.990$ for Fig. 4A (b), inset. We then examined the reversibility of the fluoride sensor using carry-over potentiometric experiment performed upon increasing and decreasing fluoride concentration using 0.1–100 mM NaF solutions. As illustrated in Fig. 4B, the spandex fluoride sensor exhibits an excellent reversibility and repeatability of fluoride detection, with nearly identical near-Nernstian sensitivity for increasing and decreasing fluoride concentrations (*i.e.* 0.1–100 mM and reverse). Such attractive reversible response characteristics are highly promising for an advanced application requiring continuous fluoride monitoring (Jayeoye and Rujiralai,

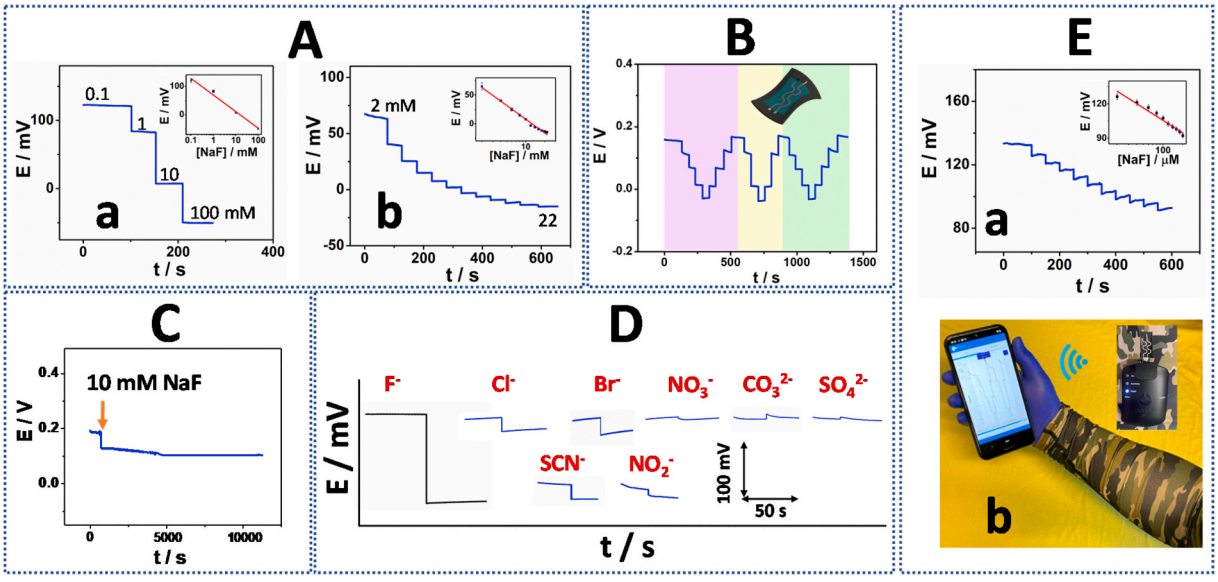

Fig. 4. Evaluation of potentiometric sensing performance of the solid-contact spandex fluoride sensor. (A)Fluoride sensing performance over the concentration range of- (a) 0.1–100 mM and (b) 2–22 mM NaF solutions. Insets present the respective calibration plots; respective error bars shown are each based on three independent measurements, n = 3, RSD = 1.67% and 1.45%, respectively. (B) Carry-over analysis over the concentration range of 0.1–100 mM NaF solutions. (C) Stability evaluation over 3.5 h in 10 mM NaF solution. (D) Interferents study while changing the concentration of the different tested anions from 1 to 10 mM. (E) Fluoride sensing performance over the concentration range of- (a) 20–200 µM. The inset presents the corresponding calibration plot; error bars shown are based on three independent measurements, n = 3, RSD = 1.81%. (b) Image depicting wireless interfacing between the spandex fluoride sensor and a nearby smartphone (displaying the sensor reversibility) via the portable potentiostat for real-time fluoride detection.

2020; Kono et al., 1987; Levin et al., 2016; Xing et al., 2020). In order to estimate the limit of detection (LOD) and lower limit of quantification (LOQ) of the spandex fluoride sensor, open-circuit potentiometric measurements were performed via 20 μM NaF concentration increments [Fig. 4E (a)]. The spandex fluoride sensor displays a well-defined potentiometric response for these small 20 μM concentration changes up to 200 μM. The calibration plot, presented as the inset, displays near-Nernstian fluoride response, corresponding to $E = -58.77 \log_{10}[NaF] + 181.26$ mV, $R^2 = 0.974$ for Fig. 4E (a), inset. An LOD [calculated as 3 × (SD of y-intercept/slope)] of 17 μM was estimated based on these favorable signal-to-noise characteristics. Such low LOD reflects the ability of the developed textile sensor to detect 1.7 nmol of fluoride (considering the 100 μL sample volume), which assuming the complete biocatalytic hydrolysis of the G-type nerve agent, can be translated to 0.24 μg and 0.3 μg of sarin and soman (target fluorine-containing G-type nerve agents), respectively. Based on the general human lethal concentration threshold (Lct50) values for 2-min air exposure times of sarin and soman - which are both around 390–420 μg/min (Lukey et al., 2019) - and considering the fast response of the developed textile sensor (50 s), the sensor can potentially provide a timely alert on exposure to such chemical threats.

The stability of the solid-contact spandex fluoride sensor was evaluated first in a 10 mM NaF solution over a period of 3.5 h (Fig. 4C). The sensor exhibited a sufficiently stable fluoride response over the investigated period, with a potential drift of 7 mV/h. The favorable medium-term stability can be attributed to the high low-frequency capacitance due to the CNT-COOH intermediate layer (Parra et al., 2009; Yuan et al., 2015). Such behavior holds promise for future continuous fluoride monitoring applications. The new textile fluoride sensor can be easily detached (as shown in Fig. S2C) and thus allows convenient removal, e.g., before washing. Such easily interchangeable sensor can facilitate applications over long periods. Such long-term stability of five spandex fluoride sensors was investigated via daily monitoring of the fluoride response over a period of 7 days. The spandex fluoride sensors were stored at room temperature under dark conditions, while being incubated in 0.1 mM NaF solution (in 10 mM MES, pH 5.5). The high stability of the obtained fluoride sensitivities within 55–60 mV/decade (RSD = 7.82%, n = 5) validates the robustness of the solid-contact spandex fluoride sensor, as desired for sensing applications demanding long-term use. Finally, the selectivity of the solid-contact spandex fluoride sensor was evaluated in the presence of potentially interfering anions, including chloride, bromide, nitrate, carbonate, sulfate, thiocyanate and nitrite anions. Fig. 4D presents the relative potentiometric responses of the solid-contact fluoride sensor to various anions, with the respective anion concentrations changing from 1 mM to 10 mM. These signals demonstrate the high selectivity of the spandex fluoride sensor toward the detection of primary fluoride anions. This excellent performance is attributed to the exceptional binding affinity of Sn-based organometallic ionophores toward fluoride anions (Goud et al., 2020; Perdikaki et al., 2002). The minor yet relatively insignificant interferences from certain anions (Cl^-, Br^- and SCN^-) are expected based on their positions in the Hofmeister series, which promote weakened hydrophobic interactions and higher hydroxide ion interference within the hydrophobic F-selective membrane in aqueous medium. Lastly, Fig. S2 presents real images of the spandex fluoride sensor- (A) during attachment, (B) after attachment and (C) during detachment from the garment (Note: We applied a silicone adhesive liquid underneath the spandex substrate for attaching the sensor to the garment). It reflects the facile attachment and detachment of the wearable spandex fluoride sensor, which allows convenient removal and storage of these sensors when not in use, along with rapid replacement of the sensor following an alert for further confirmation of the presence of ambient G-type nerve agents.

3.5. Textile-based enzymatic biosensor performance: toward detecting G-Type nerve agent simulant

Hydrolytic enzymes, particularly OPAA and OPH, have long been investigated for the detection and decontamination of nerve agents (Li et al., 2016a, 2016b; Simonian et al, 1999, 2001). It has thereby been established that OPAA offers highly specific catalytic activity toward fluorine-containing G-type nerve agents whereas, while OPH offers high catalytic activity toward a broad spectrum of nerve agents including common organophosphates (Simonian et al, 1999, 2001). Accordingly, the use of an OPAA/F biosensor chip for the *in vitro* detection of the G-type nerve-agent simulant DFP was described recently (Goud et al., 2020). The structural similarity between DFP and fluorine-containing G-type neurotoxins has made it a useful analogue for evaluating biosensing technologies for these chemical warfare agents. Here, we demonstrate the biosensing performance of enzyme-modified fluoride textile sensors in DFP resulting from connection to its biocatalytic hydrolysis in the presence of immobilized OPAA and OPH enzymes. Details of immobilization of the enzymes on the fluoride textile transducers are given in the Supplementary Information. The influence of pH on the Sn-based fluoride ionophore activity has been investigated in our previous work and the optimal fluoride response was found to be at pH 5.5. However, to achieve a balance between the effective fluoride recognition and enzyme activities, we have selected pH 6.8 as the optimal pH for DFP biosensing (Goud et al., 2020). Fig. 5A (left) displays the DFP biosensing response for the OPAA-modified spandex fluoride sensors (OPAA-F sensors) compared to the non-enzymatic fluoride response to DFP (negative control), over a DFP concentration range of 250–2500 μM. The corresponding calibration plot is also presented (Fig. 5A, right). A sensitive (25.11 μV/μM DFP) and nearly linear ($R^2 = 0.987$) response to DFP was obtained with the OPAA-F textile sensor ($E = -0.025$ [DFP] + 208.67 mV) compared to the negligible response observed for the control sensor. Such sensitive DFP biosensing response benefits from the high catalytic activity of OPAA toward DFP (Simonian et al., 2001).

DFP biosensing capability was also demonstrated by employing OPH-modified spandex fluoride sensors (OPH–F sensors). Fig. 5B (left) presents the DFP biosensing response for the OPH-F sensors along with the non-enzymatic fluoride response to DFP (negative control), over the DFP concentration range of 250–2750 μM. The corresponding calibration plot, presented in Fig. 5B (right) shows a sensitive (37.87 μV/μM DFP) and linear ($R^2 = 0.998$) response to DFP with the OPH-F sensors ($E = -0.038$ [DFP] + 180.71 mV), while a negligible response was observed using the non-enzymatic fluoride sensor. Similar to that of the OPAA-F sensor, the sensitive DFP biosensing response can be ascribed to the high catalytic activity of OPH toward DFP (Simonian et al, 1999, 2001).

Finally, DFP biosensing experiments were performed with the OPAA-F sensors and the OPH-F sensors using lower concentrations of 50–600 μM and 50–250 μM, respectively, to determine their respective LOQs (Fig. S3). Based on the obtained results, LOQs of 200 μM and 50 μM of DFP were obtained for the OPAA-F and OPH-F sensors, respectively. Overall, the high sensitivity and impressive LOQs obtained with both OPAA and OPH-modified spandex fluoride sensors signify the tremendous potential for employing these wearable textile-based enzymatic DFP biosensors in diverse military applications requiring the on-site detection of fluorine-containing G-type nerve agents. Additionally, the integration of a wearable potentiostat with these wearable textile-based DFP biosensors, coupled via Bluetooth-enabled wireless interfacing to a nearby smartphone, would enable the rapid and user-friendly field detection of ambient fluorine-containing G-type nerve agents. This would ultimately boost the efficiency of on-site threat mitigation by military personnel, emergency reaction protocols and real-time wireless data transmission to distant military surveillance bases (Chen et al., 2019; Kirlikovali et al., 2020; Li et al., 2016a, 2016b).

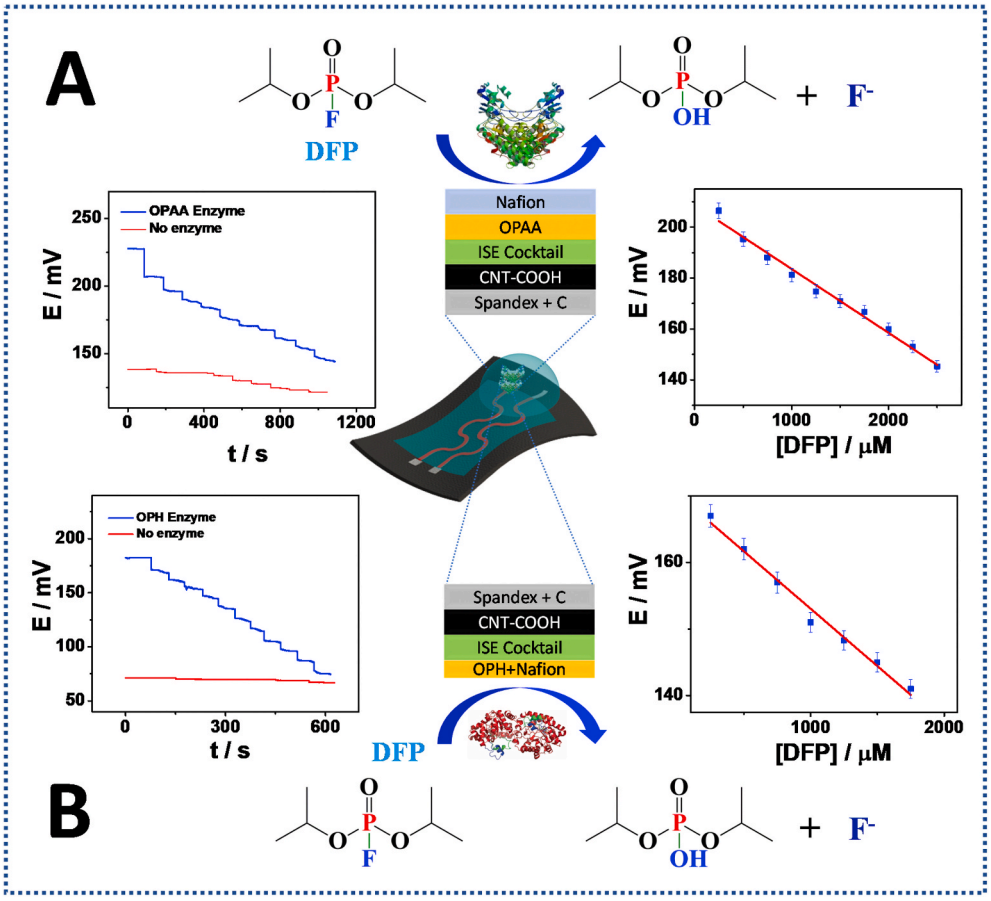

Fig. 5. Textile-based enzymatic biosensor performance toward DFP detection. (A) OPAA/F sensor performance over the concentration range of 250–2500 μM DFP solution. Adjacent graph presents the respective calibration plot; error bars shown are based on three independent measurements, n = 3, RSD = 1.52%). (B) OPH/F sensor performance over the concentration range of 250–2750 μM DFP solution. Adjacent graph presents the obtained calibration plot; error bars shown are based on three independent measurements, n = 3, RSD = 1.93%. Experiments were carried out in MES (10 mM, pH 6.8).

4. Conclusions

In this work, we have demonstrated the first example of a wearable spandex textile-based solid-contact fluoride sensor. The realization of the first wearable potentiometric fluoride sensor relied on the systematic optimization of the working electrode including the-intermediate layer, sensor design and sensor preconditioning parameters. The solid-contact spandex fluoride sensor also exhibited high selectivity, reproducibility, and reversibility. The introduction of an alternative CNT-COOH ion-to-electron transducer layer further enhanced the performance with an attractive near-Nernstian sensitivity along with a stable response. Further attention to the printed ink materials and serpentine connecting structures resulted in a superior mechanical resiliency toward severe and repeated stretching and bending deformations. The performance of the spandex fluoride potentiometric sensor enabled its translation into enzymatic textile biosensors for detecting DFP, a common simulant of F-containing G-type nerve agents. Such biosensing has been realized using OPAA and OPH enzymes, with both enzymes offering facile biocatalytic hydrolysis, thereby enabling the detection of DFP in connection to the new flexible fluoride transducer. The resulting potentiometric biosensors offer highly sensitive DFP detection. Special attention has been given to the miniaturization of the entire textile-based sensor system toward a user-friendly field operation in connection to a compact potentiostatic interface and wireless signal transmission to a nearby mobile device. Future efforts will evaluate and compare the sensitivity, selectivity and speed of the two enzymatic biosensors toward timely alert upon exposure to actual fluorine-containing G-type organophosphate neurotoxin warfare agents. These new wearable sensing capabilities are expected to boost the efficiency of on-site threat mitigation toward effective defense warning and countermeasures for protecting soldiers and civilians against threat compounds.

CRediT authorship contribution statement

K. Yugender Goud: Conceptualization, Writing – original draft. **Samar S. Sandhu:** Conceptualization, Writing – original draft. **Hazhir Teymourian:** Conceptualization, Writing – original draft. **Lu Yin:** Conceptualization, Writing – original draft. **Nicholas Tostado:** Conceptualization, Writing – original draft. **Frank M. Raushel:** Conceptualization, Writing – original draft. **Steven P. Harvey:** Conceptualization, Writing – original draft. **Lee C. Moores:** Conceptualization, Writing – original draft. **Joseph Wang:** Conceptualization, Writing – original draft.

Declaration of competing interest

The authors declare that they have no known competing financial interests or personal relationships that could have appeared to influence the work reported in this paper.

Acknowledgements

This work was supported by the U.S. Army Engineer Research and Development Center, Installation and Operation Environment Program under Contract number W912HZ-18-BAA-01 and PE 0622720. Use of trade, product or firm names in this report is for descriptive purposes only and does not imply endorsement by the U.S. Government. Permission was granted by the Director, Environmental Laboratory to publish this information. The findings of this document are not to be construed as an official Department of the Army position unless so designated by other authorized documents. The SEBS (MD 1648) copolymer used in this work was provided by Kraton Corp.

Appendix A. Supplementary data

Supplementary data to this article can be found online at https://doi.org/10.1016/j.bios.2021.113172.

References

Bae, S.Y., Myslinski, J.M., McMahon, L.R., Height, J.J., Bigley, A.N., Raushel, F.M., Harvey, S.P., 2018. An OPAA enzyme mutant with increased catalytic efficiency on the nerve agents sarin, soman, and GP. Enzym. Microb. Technol. 112, 65–71. https://doi.org/10.1016/j.enzmictec.2017.11.001.

Bandodkar, A.J., Hung, V.W.S., Jia, W., Valdés-Ramírez, G., Windmiller, J.R., Martinez, A.G., Ramírez, J., Chan, G., Kerman, K., Wang, J., 2013. Tattoo-based potentiometric ion-selective sensors for epidermal pH monitoring. Analyst 138 (1), 123–128. https://doi.org/10.1039/c2an36422k.

Bandodkar, A.J., Jeerapan, I., You, J.-M., Nuñez-Flores, R., Wang, J., 2016. Highly stretchable fully-printed CNT-based electrochemical sensors and biofuel cells: combining intrinsic and design-induced stretchability. Nano Lett. 16, 721–727. https://doi.org/10.1021/acs.nanolett.5b04549.

Bandodkar, A.J., Molinnus, D., Mirza, O., Guinovart, T., Windmiller, J.R., Valdés-Ramírez, G., Andrade, F.J., Schöning, M.J., Wang, J., 2014. Epidermal tattoo potentiometric sodium sensors with wireless signal transduction for continuous non-invasive sweat monitoring. Biosens. Bioelectron. 54, 603–609. https://doi.org/10.1016/j.bios.2013.11.039.

Bariya, M., Li, L., Ghattamaneni, R., Ahn, C.H., Nyein, H.Y.Y., Tai, L.-C., Javey, A., 2020. Glove-based sensors for multimodal monitoring of natural sweat. Sci. Adv. 6, eabb8308 https://doi.org/10.1126/sciadv.abb8308.

Bobacka, J., 2006. Conducting polymer-based solid-state ion-selective electrodes. Electroanalysis 18, 7–18. https://doi.org/10.1002/elan.200503384.

Bobacka, J., 1999. Potential stability of all-solid-state ion-selective electrodes using conducting polymers as ion-to-electron transducers. Anal. Chem. 71, 4932–4937. https://doi.org/10.1021/ac990497z.

Bujes-Garrido, J., Arcos-Martínez, M.J., 2017. Development of a wearable electrochemical sensor for voltammetric determination of chloride ions. Sensor. Actuator. B Chem. 240, 224–228. https://doi.org/10.1016/j.snb.2016.08.119.

Chen, Z., Ma, K., Mahle, J.J., Wang, H., Syed, Z.H., Atilgan, A., Chen, Y., Xin, J.H., Islamoglu, T., Peterson, G.W., Farha, O.K., 2019. Integration of metal–organic frameworks on protective layers for destruction of nerve agents under relevant conditions. J. Am. Chem. Soc. 141, 20016–20021. https://doi.org/10.1021/jacs.9b11172.

Crespo, G.A., Macho, S., Bobacka, J., Rius, F.X., 2009. Transduction mechanism of carbon nanotubes in solid-contact ion-selective electrodes. Anal. Chem. 81, 676–681. https://doi.org/10.1021/ac802078z.

Crespo, G.A., Macho, S., Rius, F.X., 2008. Ion-selective electrodes using carbon nanotubes as ion-to-electron transducers. Anal. Chem. 80, 1316–1322. https://doi.org/10.1021/ac071156l.

Emaminejad, S., Gao, W., Wu, E., Davies, Z.A., Yin Yin Nyein, H., Challa, S., Ryan, S.P., Fahad, H.M., Chen, K., Shahpar, Z., Talebi, S., Milla, C., Javey, A., Davis, R.W., 2017. Autonomous sweat extraction and analysis applied to cystic fibrosis and glucose monitoring using a fully integrated wearable platform. Proc. Natl. Acad. Sci. Unit. States Am. 114, 4625–4630. https://doi.org/10.1073/pnas.1701740114.

Gao, W., Emaminejad, S., Nyein, H.Y.Y., Challa, S., Chen, K., Peck, A., Fahad, H.M., Ota, H., Shiraki, H., Kiriya, D., Lien, D.-H., Brooks, G.A., Davis, R.W., Javey, A., 2016. Fully integrated wearable sensor arrays for multiplexed in situ perspiration analysis. Nature 529, 509–514. https://doi.org/10.1038/nature16521.

Garland, N.T., McLamore, E.S., Cavallaro, N.D., Mendivelso-Perez, D., Smith, E.A., Jing, D., Claussen, J.C., 2018. Flexible laser-induced graphene for nitrogen sensing in soil. ACS Appl. Mater. Interfaces 10 (45), 39124–39133. https://doi.org/10.1021/acsami.8b10991.

Goud, K.Y., Teymourian, H., Sandhu, S.S., Tostado, N., Mishra, R.K., Moore, L.C., Harvey, S.P., Wang, J., 2020. OPAA/fluoride biosensor chip towards field detection of G-type nerve agents. Sensor. Actuator. B Chem. 320, 128344. https://doi.org/10.1016/j.snb.2020.128344.

Guinovart, T., Bandodkar, A.J., Windmiller, J.R., Andrade, F.J., Wang, J., 2013. A potentiometric tattoo sensor for monitoring ammonium in sweat. Analyst 138, 7031–7038. https://doi.org/10.1039/c3an01672b.

Hassan, S.S.M., Eldin, A.G., Amr, A.E.G.E., Al-Omar, M.A., Kamel, A.H., 2019. Single-walled carbon nanotubes (SWCNTs) as solid-contact in all-solid-state perchlorate ISEs: applications to fireworks and propellants analysis. Sensors 19. https://doi.org/10.3390/s19122697.

Hu, J., Stein, A., Bühlmann, P., 2016. Rational design of all-solid-state ion-selective electrodes and reference electrodes. TrAC Trends Anal. Chem. (Reference Ed.) 76, 102–114. https://doi.org/10.1016/j.trac.2015.11.004.

Hubble, L.J., Wang, J., 2019. Sensing at your fingertips: glove-based wearable chemical sensors. Electroanalysis 31, 428–436. https://doi.org/10.1002/elan.201800743.

Jayeoye, T.J., Rujiralai, T., 2020. Sensitive and selective colorimetric probe for fluoride detection based on the interaction between 3-aminophenylboronic acid and dithiobis (succinimidylpropionate) modified gold nanoparticles. New J. Chem. 44, 5711–5719. https://doi.org/10.1039/D0NJ00897D.

Kang, Y., Kampf, J.W., Meyerhoff, M.E., 2007. Optical fluoride sensor based on monomer-dimer equilibrium of scandium(III)-octaethylporphyrin in a plasticized polymeric film. Anal. Chim. Acta 598 (2), 295–303. https://doi.org/10.1016/j.aca.2007.07.048.

Kang, Y., Lutz, C., Hong, S.A., Sung, D., Lee, J.S., Shin, J.H., Nam, H., Cha, G.S., Meyerhoff, M.E., 2010. Development of a fluoride-selective electrode based on scandium(III) octaethylporphyrin in a plasticized polymeric membrane. Bull. Kor. Chem. Soc. 31, 1601–1608.

Kim, J., Campbell, A.S., de Ávila, B.E.-F., Wang, J., 2019. Wearable biosensors for healthcare monitoring. Nat. Biotechnol. 37, 389–406. https://doi.org/10.1038/s41587-019-0045-y.

Kirlikovali, K.O., Chen, Z., Islamoglu, T., Hupp, J.T., Farha, O.K., 2020. Zirconium-based metal–organic frameworks for the catalytic hydrolysis of organophosphorus nerve agents. ACS Appl. Mater. Interfaces 12, 14702–14720. https://doi.org/10.1021/acsami.9b20154.

Kirsch, J., Siltanen, C., Zhou, Q., Revzin, A., Simonian, A., 2013. Biosensor technology: recent advances in threat agent detection and medicine. Chem. Soc. Rev. 42, 8733–8768. https://doi.org/10.1039/c3cs60141b.

Kono, K., Yoshida, Y., Yamagata, H., Watanabe, M., Shibuya, Y., Doi, K., 1987. Urinary fluoride monitoring of industrial hydrofluoric acid exposure. Environ. Res. 42, 415–420. https://doi.org/10.1016/S0013-9351(87)80208-6.

Lee, Y., Howe, C., Mishra, S., Lee, D.S., Mahmood, M., Piper, M., Kim, Y., Tieu, K., Byun, H.-S., Coffey, J.P., Shayan, M., Chun, Y., Costanzo, R.M., Yeo, W.-H., 2018. Wireless, intraoral hybrid electronics for real-time quantification of sodium intake toward hypertension management. Proc. Natl. Acad. Sci. Unit. States Am. 115, 5377–5382. https://doi.org/10.1073/pnas.1719573115.

Levin, S., Krishnan, S., Rajkumar, S., Halery, N., Balkunde, P., 2016. Monitoring of fluoride in water samples using a smartphone. Sci. Total Environ. 551–552, 101–107. https://doi.org/10.1016/j.scitotenv.2016.01.156.

Li, P., Moon, S.-Y., Guelta, M.A., Harvey, S.P., Hupp, J.T., Farha, O.K., 2016a. Encapsulation of a nerve agent detoxifying enzyme by a mesoporous zirconium metal–organic framework engenders thermal and long-term stability. J. Am. Chem. Soc. 138, 8052–8055. https://doi.org/10.1021/jacs.6b03673.

Li, P., Moon, S.-Y., Guelta, M.A., Lin, L., Gómez-Gualdrón, D.A., Snurr, R.Q., Harvey, S. P., Hupp, J.T., Farha, O.K., 2016b. Nanosizing a metal–organic framework enzyme carrier for accelerating nerve agent hydrolysis. ACS Nano 10, 9174–9182. https://doi.org/10.1021/acsnano.6b04996.

Liu, K., Jiang, X., Song, Y., Liang, R., 2019. Robust fabrication of nanomaterial-based all-solid-state ion-selective electrodes. RSC Adv. 9, 16713–16719. https://doi.org/10.1039/c9ra02770j.

Liu, Yueling, Liu, Yunzhong, Meng, Z., Qin, Y., Jiang, D., Xi, K., Wang, P., 2020. Thiol-functionalized reduced graphene oxide as self-assembled ion-to-electron transducer for durable solid-contact ion-selective electrodes. Talanta 208, 120374. https://doi.org/10.1016/j.talanta.2019.120374.

Lukey, B.J., Romano, J.A., Harry, S., 2019. Chemical Warfare Agents, Persepsi Masyarakat Terhadap Perawatan Ortodontik Yang Dilakukan Oleh Pihak Non Profesional. CRC Press. https://doi.org/10.1201/9781498769235.

Min, J., Sempionatto, J.R., Teymourian, H., Wang, J., Gao, W., 2021. Wearable electrochemical biosensors in North America. Biosens. Bioelectron. 172, 112750. https://doi.org/10.1016/j.bios.2020.112750.

Mishra, R.K., Barfidokht, A., Karajic, A., Sempionatto, J.R., Wang, Joshua, Wang, Joseph, 2018. Wearable potentiometric tattoo biosensor for on-body detection of G-type nerve agents simulants. Sensor. Actuator. B Chem. 273, 966–972. https://doi.org/10.1016/j.snb.2018.07.001.

Mitchell-Koch, J.T., Pietrzak, M., Malinowska, E., Meyerhoff, M.E., 2006. Aluminum(III) porphyrins as ionophores for fluoride selective polymeric membrane electrodes. Electroanalysis 18, 551–557. https://doi.org/10.1002/elan.200503450.

Mousavi, Z., Bobacka, J., Lewenstam, A., Ivaska, A., 2009. Poly(3,4-ethylenedioxythiophene) (PEDOT) doped with carbon nanotubes as ion-to-electron transducer in polymer membrane-based potassium ion-selective electrodes. J. Electroanal. Chem. 633, 246–252. https://doi.org/10.1016/j.jelechem.2009.06.005.

Mousavi, Z., Teter, A., Lewenstam, A., Maj-Zurawska, M., Ivaska, A., Bobacka, J., 2011. Comparison of multi-walled carbon nanotubes and poly(3-octylthiophene) as ion-to-electron transducers in all-solid-state potassium ion-selective electrodes. Electroanalysis 23, 1352–1358. https://doi.org/10.1002/elan.201000747.

Parra, E.J., Crespo, G.A., Riu, J., Ruiz, A., Rius, F.X., 2009. Ion-selective electrodes using multi-walled carbon nanotubes as ion-to-electron transducers for the detection of perchlorate. Analyst 134, 1905. https://doi.org/10.1039/b908224g.

Parrilla, M., Cánovas, R., Jeerapan, I., Andrade, F.J., Wang, J., 2016. A textile-based stretchable multi-ion potentiometric sensor. Adv. Healthc. Mater. 5, 996–1001. https://doi.org/10.1002/adhm.201600092.

Parrilla, M., Cuartero, M., Padrell Sánchez, S., Rajabi, M., Roxhed, N., Niklaus, F., Crespo, G.A., 2019. Wearable all-solid-state potentiometric microneedle patch for intradermal potassium detection. Anal. Chem. 91, 1578–1586.

Perdikaki, K., Tsagkatakis, I., Chaniotakis, N.A., Altmann, R., Jurkschat, K., Reeske, G., 2002. Selective fluoride recognition and potentiometric properties of ion-selective electrodes based on bis(halodiphenylstannyl)alkanes. Anal. Chim. Acta 467, 197–204. https://doi.org/10.1016/S0003-2670(02)00534-2.

Ramanathan, M., Wang, L., Wild, J.R., Meyeroff, M.E., Simonian, A.L., 2010. Monitoring of diisopropyl fluorophosphate hydrolysis by fluoride-selective polymeric films using absorbance spectroscopy. Anal. Chim. Acta 667 (1–2), 119–122. https://doi.org/10.1016/j.aca.2010.04.006.

Ray, T.R., Choi, J., Bandodkar, A.J., Krishnan, S., Gutruf, P., Tian, L., Ghaffari, R., Rogers, J.A., 2019. Bio-Integrated wearable systems: a comprehensive review. Chem. Rev. 119, 5461–5533. https://doi.org/10.1021/acs.chemrev.8b00573.

Sempionatto, J.R., Nakagawa, T., Pavinatto, A., Mensah, S.T., Imani, S., Mercier, P., Wang, J., 2017. Eyeglasses based wireless electrolyte and metabolite sensor platform. Lab Chip 17, 1834–1842. https://doi.org/10.1039/c7lc00192d.

Shao, Y., Ying, Y., Ping, J., 2020. Recent advances in solid-contact ion-selective electrodes: functional materials, transduction mechanisms, and development trends. Chem. Soc. Rev. 49, 4405–4465. https://doi.org/10.1039/C9CS00587K.

Simonian, A., DiSioudi, B., Wild, J., 1999. An enzyme based biosensor for the direct determination of diisopropyl fluorophosphate. Anal. Chim. Acta 389, 189–196. https://doi.org/10.1016/S0003-2670(99)00170-1.

Simonian, A., Grimsley, J., Flounders, A., Schoeniger, J., Cheng, T.-C., DeFrank, J., Wild, J., 2001. Enzyme-based biosensor for the direct detection of fluorine-containing organophosphates. Anal. Chim. Acta 442, 15–23. https://doi.org/10.1016/S0003-2670(01)01131-X.

Simonian, A.L., Flounders, A.W., Wild, J.R., 2004. FET-based biosensors for the direct detection of organophosphate neurotoxins. Electroanalysis 16 (22), 1896–1906. https://doi.org/10.1002/elan.200403078.

Tsai, P.C., Fox, N., Bigley, A.N., Harvey, S.P., Barondeau, D.P., Raushel, F.M., 2012. Enzymes for the homeland defense: optimizing phosphotriesterase for the hydrolysis of organophosphate nerve agents. Biochemistry 51 (32), 6463–6475. https://doi.org/10.1021/bi300811t.

Wang, Lie, Wang, Liyuan, Zhang, Y., Pan, J., Li, S., Sun, X., Zhang, B., Peng, H., 2018. Weaving sensing fibers into electrochemical fabric for real-time health monitoring. Adv. Funct. Mater. 28, 1804456. https://doi.org/10.1002/adfm.201804456.

Windmiller, J.R., Wang, J., 2013. Wearable electrochemical sensors and biosensors: a review. Electroanalysis 25 (1), 29–46. https://doi.org/10.1002/elan.201200349.

Xing, Y., Zhu, Q., Zhou, X., Qi, P., 2020. A dual-functional smartphone-based sensor for colorimetric and chemiluminescent detection: a case study for fluoride concentration mapping. Sensor. Actuator. B Chem. 319, 128254. https://doi.org/10.1016/j.snb.2020.128254.

Xu, J., Zhang, Z., Gan, S., Gao, H., Kong, H., Song, Z., Ge, X., Bao, Y., Niu, L., 2020. Highly stretchable fiber-based potentiometric ion sensors for multichannel real-time analysis of human sweat. ACS Sens. 5 (9), 2834–2842. https://doi.org/10.1021/acssensors.0c00960.

Yin, L., Kumar, R., Karajic, A., Xie, L., You, J., Joshuia, D., Lopez, C.S., Miller, J., Wang, J., 2018. From all-printed 2D patterns to free-standing 3D structures: controlled buckling and selective bonding. Adv. Mater. Technol. 3, 1800013. https://doi.org/10.1002/admt.201800013.

Yin, L., Scharf, J., Ma, J., Doux, J.-M., Redquest, C., Le, V.L., Yin, Y., Ortega, J., Wei, X., Wang, J., Meng, Y.S., 2021. High performance printed AgO-Zn rechargeable battery for flexible electronics. Joule 5, 228–248. https://doi.org/10.1016/j.joule.2020.11.008.

Yuan, D., Anthis, A.H.C., Ghahraman Afshar, M., Pankratova, N., Cuartero, M., Crespo, G.A., Bakker, E., 2015. All-solid-State potentiometric sensors with a multiwalled carbon nanotube inner transducing layer for anion detection in environmental samples. Anal. Chem. 87, 8640–8645. https://doi.org/10.1021/acs.analchem.5b01941.